ORIGINAL ARTICLE

Metabolic stratification driven by surface and subsurface interactions in a terrestrial mud volcano

Ting-Wen Cheng[1,7], Yung-Hsin Chang[1], Sen-Lin Tang[2], Ching-Hung Tseng[2], Pei-Wen Chiang[2], Kai-Ti Chang[2], Chih-Hsien Sun[3], Yue-Gau Chen[1], Hung-Chi Kuo[4], Chun-Ho Wang[5], Pao-Hsuan Chu[1], Sheng-Rong Song[1], Pei-Ling Wang[6,7] and Li-Hung Lin[1,7]

[1]Department of Geosciences, National Taiwan University, Taipei, Taiwan; [2]Biodiversity Research Center, Academia Sinica, Taipei, Taiwan; [3]Exploration and Development Research Institute, CPC Corporation Taiwan, Miao-Li, Taiwan; [4]Department of Atmospheric Sciences, National Taiwan University, Taipei, Taiwan; [5]Institute of Earth Sciences, Academia Sinica, Taipei, Taiwan and [6]Institute of Oceanography, National Taiwan University, Taipei, Taiwan

Terrestrial mud volcanism represents the prominent surface geological feature, where fluids and hydrocarbons are discharged along deeply rooted structures in tectonically active regimes. Terrestrial mud volcanoes (MVs) directly emit the major gas phase, methane, into the atmosphere, making them important sources of greenhouse gases over geological time. Quantification of methane emission would require detailed insights into the capacity and efficiency of microbial metabolisms either consuming or producing methane in the subsurface, and establishment of the linkage between these methane-related metabolisms and other microbial or abiotic processes. Here we conducted geochemical, microbiological and genetic analyses of sediments, gases, and pore and surface fluids to characterize fluid processes, community assemblages, functions and activities in a methane-emitting MV of southwestern Taiwan. Multiple lines of evidence suggest that aerobic/anaerobic methane oxidation, sulfate reduction and methanogenesis are active and compartmentalized into discrete, stratified niches, resembling those in marine settings. Surface evaporation and oxidation of sulfide minerals are required to account for the enhanced levels of sulfate that fuels subsurface sulfate reduction and anaerobic methanotrophy. Methane flux generated by *in situ* methanogenesis appears to alter the isotopic compositions and abundances of thermogenic methane migrating from deep sources, and to exceed the capacity of microbial consumption. This metabolic stratification is sustained by chemical disequilibria induced by the mixing between upward, anoxic, methane-rich fluids and downward, oxic, sulfate-rich fluids.
The ISME Journal (2012) **6**, 2280–2290; doi:10.1038/ismej.2012.61; published online 28 June 2012
Subject Category: geomicrobiology and microbial contributions to geochemical cycles
Keywords: metabolic stratification; terrestrial mud volcano; sulfate-to-methane transition zone; methanogenesis; 16S rRNA gene clone library; metagenome

Introduction

Mud volcanoes (MVs) and hydrocarbon seepages are ubiquitous in both marine and terrestrial environments. They are characterized by continuous or episodic discharges of gaseous fluids with unconsolidated, fine-grained sediments generated during clay dehydration, compaction dewatering or tectonic pressurization at depth (Kopf, 2004). These surface expressions often represent the outlet of fluid conduits that tap into deep petroleum and natural gas reservoirs, thereby providing an accessible window to probe the characteristics of petroleum and gas sources, and the deep biosphere. Methane appears to be the major gaseous constituent released from most MVs. Recent estimates indicate that MVs and seepages onshore and offshore around the world might account for approximately 30% of the methane emission from natural sources (Etiope et al., 2008). Considering the huge capacity of methane potentially stored in the subterranean or subseafloor strata (Milkov, 2004), these geological sources might have been an important factor diverting the redox equilibrium in the atmosphere over geological time. Terrestrial MVs particularly have a vital role as methane and other hydrocarbons are directly released into the atmosphere. Therefore, any assessment of the greenhouse effect on a global scale has to consider the contribution of terrestrial MVs.

Stable isotopic and molecular compositions of hydrocarbons have been broadly utilized to identify the hydrocarbon origin and to trace the hydrocarbon migration (Whiticar, 1990; Etiope *et al.*, 2009; Sun *et al.*, 2010). On the basis of $\delta^{13}C$-CH_4 and δ^2H-CH_4 values, about 25% out of 143 studied MVs around the world release microbial methane or a mixture of microbial and thermogenic methane (Etiope *et al.*, 2009). In contrast, a plot of the same data set on the $\delta^{13}C$-CH_4 versus $C_1/(C_2 + C_3)$ diagram shows that most terrestrial MVs produce gas signals falling within an ambiguous sector due to post-genetic processes, such as microbial oxidation, mixing or molecular fractionation during migration (Etiope *et al.*, 2009). This contradictory interpretation illustrates the complexity in the identification of gas origin, as well as strengthens the importance of the post-formational microbial process at shallow depths.

Only limited studies have been conducted to investigate microbial activities and community structures in terrestrial, methane-rich MVs (Alain *et al.*, 2006; Chang *et al.*, 2012; Wrede *et al.*, 2012). These studies reveal that archaeal communities are primarily composed of anaerobic methanotrophs (ANME groups for ANaerobic Methanotrophic Euryarchaeota) with different fractions of methanogens or Crenarchaeota. Bacterial communities consist of diverse members taxonomically distributed across various phyla. The rates of methanogenesis and sulfate reduction, however, outnumber those of anaerobic oxidation of methane (AOM) by one to two orders of magnitude (Alain *et al.*, 2006). In addition, the correlation between geochemical profiles and community assemblages for sediments collected from the mud platform surrounding a bubbling pool suggests that AOM might be coupled to metal reduction (Chang *et al.*, 2012). These results demonstrate a variety of potential electron-accepting processes involved in organic degradation and/or methanotrophy, and are in contrast with the predominance of ANME members and sulfate reducers, and high sulfate-dependent methanotrophic activities in marine hydrocarbon seepages (Boetius *et al.*, 2000; Orphan *et al.*, 2002; Treude *et al.*, 2005; Knittel and Boetius, 2009). In terrestrial settings, sulfate abundances are generally much lower than in seawater. Whether sulfate-dependent metabolisms are active and how methane-related metabolisms interact with the imposed geochemical context in terrestrial MVs are not clear.

This study aimed to uncover the key microbial and abiotic processes associated with the subsurface–surface interactions that shaped the cycling of methane and other related compounds in terrestrial, methane-rich MVs. Using samples collected from the Shin-Yan-Ny-Hu MVs (SYNHMV) in southwestern Taiwan, geochemistry of pore water and gases, 16S rRNA gene diversity, abundance of functional genes extracted from metagenome data and culturing were integrated to constrain the spectrum of metabolic capability along a vertical profile.

Materials and methods

Study site and sample collection

The SYNHMV is located in the Yan-Chou area of southwestern Taiwan (Supplementary Information and Supplementary Figure S1) and comprises a cone-shaped structure (SYNH01) and a bubbling mud pool (SYNH02) (Figure 1). Muddy fluids mixed with abundant hydrocarbon gases are discharged out of the cone and pool, and drained toward the topographic depression. The fluid flux varies from time to time on the basis of visual inspection.

The majority of samples were collected from the bubbling pool SYNH02 and its surrounding mud platform. Two field campaigns were conducted in 2007 and 2009. Before sample collection, several parameters (including temperature, conductivity, redox potential and pH) of bubbling and surface fluids were measured on site using the portable probes (WTW Multi 340i, Weilheim, Germany). Samples were collected from sediments retrieved by push-coring (core c1 in 2007, cores c2 and c3 in 2009), and from bubbling fluids (ew01 and ew02 in 2009) and surface fluids along an outflow channel (sw01 to sw06 in 2009) (Figure 1). Core c1 was retrieved for pilot analyses of anions and methane. Core c2 was used for detailed analyses of aqueous, gas and isotope geochemistry, whereas core c3 was used for incubation experiments and molecular analyses. All samples were processed in the field, stored in sterile containers with/without preservatives and shipped back to the laboratory either on dry ice (samples for molecular analyses) or at ambient temperature (samples for aqueous and gas chemistry and incubations). Detailed descriptions for sample processing and geochemical analyses can be found in Supplementary Information.
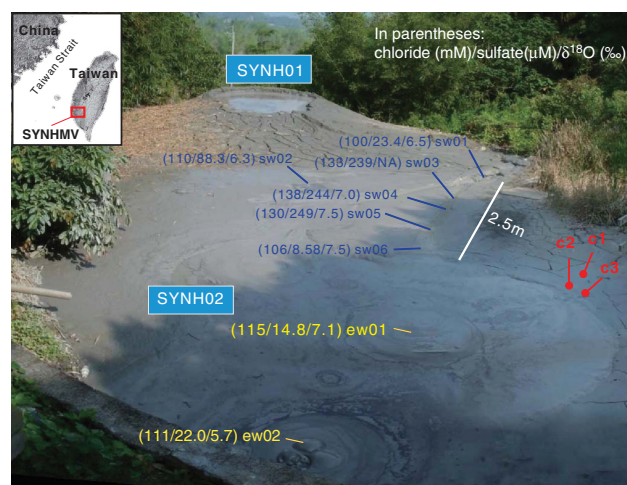

Figure 1 Field image of the SYNHMV (viewed toward northwest). Samples are categorized into cores (labeled 'c' in red), bubbling fluids (labeled 'ew' in yellow) and surface fluids in an outflow channel (labeled 'sw' in blue). The prominent geochemical features (including chloride (mM), sulfate (μM) and $\delta^{18}O$ (‰ VSMOW)) are shown in parentheses.

16S rRNA gene analysis
Genomic DNA for 16S rRNA gene analyses was extracted from 10-g sediments (from 1, 7, 11, 23 and 31 cm of core c3) and the bubbling fluid (ew01), using the UltraClean Mega Soil DNA Isolation Kit (MoBio Laboratories, Carlsbad, CA, USA) according to the manufacturer's instruction, and stored at −20 °C. Nearly complete 16S rRNA gene sequences were amplified on a Robocycler (Stratagene, La Jolla, CA, USA), using a bacterial forward primer B27F and a universal reverse primer U1492R for bacteria (Lane, 1991), and an archaeal forward primer A8F and a universal reverse primer U1513r for archaea (Huber *et al.*, 2002). The PCR protocol and downstream approaches for purification of PCR products, cloning and sequencing were described previously (Lin *et al.*, 2006). The obtained sequences were checked for chimera formation using Pintail (Ashelford *et al.*, 2005). Sequences sharing $\geqslant 98\%$ pairwise sequence identity were assigned to the same phylotype, and the nearest relative of each phylotype was retrieved from NCBI using the BLAST tool. The accession numbers of the obtained sequences deposited in GenBank were from JQ245511–JQ245695.

Metagenomic analysis
Genomic DNA in sediments from 3, 13, 23 and 31 cm of core c3 was obtained through phenol–chloroform extraction, and amplified using the Illustra Genomiphi V2 DNA Amplification Kit (GE Healthcare, Piscataway, NJ, USA). A total of 5 µg of the amplified DNA was sent to the Mission Biotech (Taipei, Taiwan) for high throughput pyrosequencing by a Roche 454 Genome Sequencer Titanium System (Roche/454 Life Sciences, Branford, CT, USA). The sequences were assembled with 99% identity in the overlapping region (40 bases) using the manufacturer's assembler. To compare the numbers of key functional genes, R (v.2.10.1; RDC Team, 2008) and the built-in statistic package were used to perform a clustering analysis. Genes subject to further analyses include *apr* (encoding adenosine-5′-phosphosulfate reductase), *dsr* (encoding dissimilatory sulfite reductase), *mcr* (encoding methyl coenzyme M reductase) and *mmo/pmo* (encoding soluble and particulate methane monooxygenase). The read counts of each gene from different depths were calculated and standardized by the Z-score method (Supplementary Information). Sequences obtained in this study were deposited in the NCBI Short Read Archive with the accession numbers of SRR389126 (31 cm), SRR389127 (23 cm), SRR389128 (13 cm) and SRR389129 (3 cm).

Incubation experiment
Sediments (5 ml or 8–10 g) collected by cutoff syringes were inoculated into serum bottles (59 ml) containing the designated medium adjusted to the local salinity (20 ml; ingredients include 5.8 g NaCl, 0.4 g $MgCl_2.6H_2O$, 0.3 g KCl, 0.15 g $CaCl_2.2H_2O$, 0.27 g NH_4Cl and 0.2 g KH_2PO_4 per liter of medium at pH 7.2) and flushed with pure argon for 2 min on site. The mineral solution was supplied with 10 mM sulfate for sulfate reduction or sulfate-dependent AOM, 5 mM acetate for acetoclastic methanogenesis and 5 mM methanol and methylamine each for methylotrophic methanogenesis. Bicarbonate at a final concentration of 10 mM was supplied for aerobic methanotrophy. Specific gases were provided for target metabolisms back in the laboratory. For aerobic methane oxidation, the headspace was flushed with air with a total volume five times the headspace volume ($\sim$35 ml), and provided with 3 ml 100% methane (equivalent to $\sim$8200 Pa). For sulfate reduction, and acetoclastic and methylotrophic methanogenesis, the headspace gas was replaced with pure nitrogen. For hydrogenotrophic methanogenesis, the headspace gas was replaced with a gas mixture of 90% H_2 and 10% CO_2. Samples for AOM were flushed with pure nitrogen first, and supplied with 5 ml ^{13}C-labeled methane (equivalent to $\sim$13 000 Pa). The incubations were performed at room temperature ($\sim$25 °C) in the dark. Methane, sulfate and $^{13}CO_2$ were monitored for methanogenesis/aerobic methanotrophy, sulfate reduction and AOM through time, respectively. The accumulated yields of methane in the methanogenic incubations were further plotted against time to derive the initial methane production rate (within 3 days) used to constrain the maximum *in situ* methanogenic activity.

Quantification of consumption and production rates of sulfate and methane
The general diagenetic equation for reactive transport was used to model the solute transport and microbial reaction rate in the sediment column:

$$\frac{\partial C_i}{\partial t} = \phi D_{sed} \frac{\partial^2 C_i}{\partial z^2} - \phi v \frac{\partial C_i}{\partial z} + R_i \qquad (1)$$

where C_i is the solute species i of interest, t is the time, z is the depth, φ is the porosity, D_{sed} is the diffusivity corrected for tortuosity, v is the advection rate, and R is the net reaction rate. Concentration and porosity data used in the modeling were adopted from the measurements. The correction of diffusivity for tortuosity followed the empirical relationships reported previously (Wang *et al.*, 2008b). The modeling further assumed that sedimentation and compaction rates were zero and a steady state was reached within a definitive time scale so the term $\partial C_i/\partial t$ was zero. The programs (NRR1 and NRR2) developed by Wang *et al.* (2008b) were employed to derive the predicted concentrations and net reaction rates for sulfate and methane.

Given that chloride is soluble and inert to most abiotic and biological reactions in ambient environments, the reaction term (R_i) for chloride in the general diagenetic equation could be omitted. The
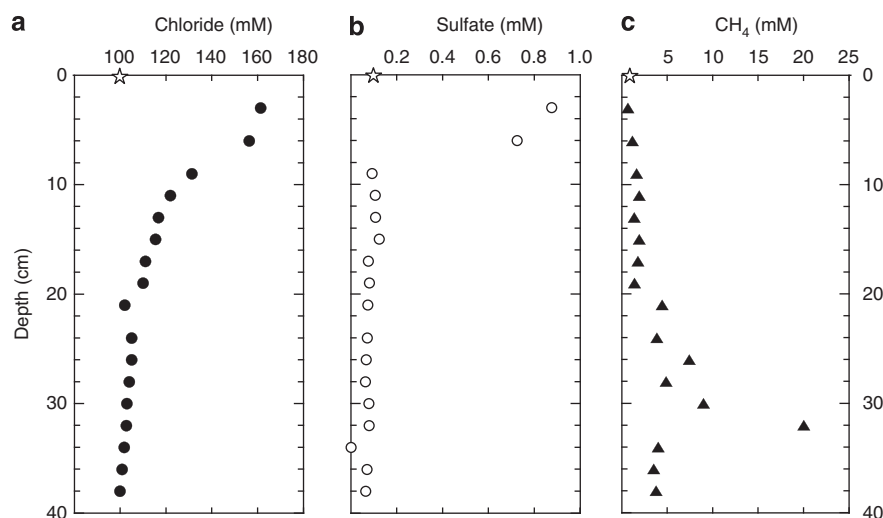
Figure 2 Concentrations of chloride (**a**), sulfate (**b**), and methane (**c**) in pore water of core c1 collected in 2007. Open-star symbols represent the compound concentrations in the bubbling fluid.

chloride profile was then used to compute the advection rate. Integration over diffusion and advection terms demonstrated that chloride varied exponentially with depth. The best fit to the observed chloride profile required fluid advection at a rate of 0.10 ± 0.03 m per year. However, the profile predicted simply by diffusion and advection transport could not replicate the observed chloride concentrations at shallow depths. This is most likely because evaporation at the surface and shallow depths enhances solute concentrations. The net reaction rates for sulfate and methane were further calculated using the advection rate of 0.1 m per year.

Results

Geochemical characteristics
The bubbling fluid with a temperature of 23.6 °C was alkaline (pH 8.36), reducing (E_h −340 mV), moderately saline (~110 mM chloride) and low in sulfate (<30 μM; Figure 1 and Supplementary Table S1). Sulfate (8.6–249 μM) and chloride (100–138 mM) concentrations in the surface fluids along an outflow channel were variable. The $\delta^{18}O$ values of the bubbling and surface fluids spanned from 6.3 to 7.5‰ (Figure 1), a range greater than those of local meteoric water and similar to those of the bubbling fluids collected from other MVs in southwestern Taiwan (Supplementary Figure S2). Methane concentrations in the bubbling fluids ranged from 0.7 to 0.9 mM (roughly equivalent to 50–64% partial pressure of methane in the gas phase). The $\delta^{13}C$ values of methane in the bubbling fluid were around −34.5‰ (Supplementary Table S1). Ethane and propane concentrations in the bubbling fluids were from 28 to 31 μM and from 8.6 to 9.3 μM, respectively.

Pilot analyses of pore water samples collected in 2007 showed that sulfate and chloride concentrations decreased with depth (Figure 2). Although sulfate was nearly depleted below 9 cm, chloride concentrations decreased from 161 mM at the top to 100 mM at 38 cm. In contrast, methane concentrations increased with depth and peaked at 32 cm (20 mM). These data showing a sulfate-methane transition zone (SMTZ) at 9–20 cm prompted detailed geochemical analyses of samples collected in 2009. Chloride and sulfate profiles in 2009 (Figure 3 and Supplementary Table S2) exhibited a pattern similar to those in 2007. Chloride concentrations gradually decreased with depth. Sulfate concentrations decreased from 4.1 mM at the top to <10 μM at depths below 10 cm. The depletion of sulfate was accompanied with an increase of methane. Below ~20 cm, the methane concentrations varied substantially between 1.29 and 2.14 mM. The $\delta^{13}C$ values of methane decreased from −39‰ at the top to −48‰ at the deepest interval. Ethane concentrations remained at a nearly constant level over most depth intervals, whereas propane concentrations decreased with depth. Both ethane and propane concentrations were one to two orders of magnitude less than those of methane. Although alkalinity decreased with depth, the $\delta^{13}C$ values of dissolved inorganic carbon exhibited a U-shaped profile with the lowest value of 4.3‰ at the SMTZ and the high values of 7.1–7.3‰ at the deepest and top intervals.

Compositions of 16 S rRNA gene
A total of 402 archaeal and 668 bacterial 16S rRNA gene clone sequences were obtained from the bubbling fluid and sediments, and clustered into 36 and 149 phylotypes (98% similarity cutoff), respectively (Figure 4 and Supplementary Table S3). Of the archaeal members, >60% of any individual library comprised sequences affiliated with methanogens (Figure 4). The majority of methanogens related to these sequences switched from Methanosarcinales (*Methanosaeta*- and *Methanolobus*-related strains) at ≤7 cm to Methanomicrobiales (*Methanoculleus*- and
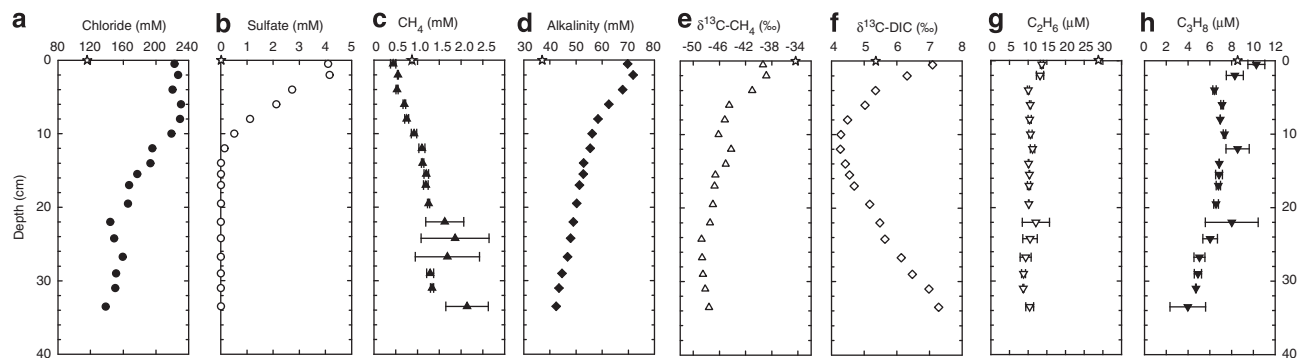
Figure 3 Concentrations of chloride (**a**), sulfate (**b**), methane (**c**), and alkalinity (**d**), carbon isotopic compositions of methane (**e**) and DIC (**f**), and concentrations of ethane (**g**) and propane (**h**) in pore water of core c2 collected in 2009. DIC stands for dissolved inorganic carbon. Gas abundances in (**c**), (**g**) and (**h**) were averaged over triplicate samples from the same intervals. The error bar represents one s.d. Open-star symbols represent the compound concentrations in the bubbling fluid.

Methanocalculus-related strains) at $\geqslant 11$ cm. Some archaeal sequences (1–9%) in the bubbling fluid and at 7 cm were affiliated with the ANME-1 group.

Bacterial community assemblages varied substantially among samples (Figure 4 and Supplementary Table S3). Phylum-based categorization indicated that the decrease in Cyanobacteria and Gamma-Proteobacteria was accompanied with an increase in Firmicutes and Bacteroidetes as the depth increased. The dominant sequences (>10% of each clone library) were affiliated with hydrocarbon-degrading *Syntrophorhabdus* sp. (Qiu *et al.*, 2008) and *Alcanivorax* sp. (Wang *et al.*, 2008a), heterotrophic *Marinobacter* sp. (Zhang *et al.*, 2002), *Tindallida* sp. (Alazard *et al.*, 2007), *Pseudomonas* sp., *Clostridium* sp. (Shiratori *et al.*, 2009) and *Alkaliflexus imshenetskii* (Zhilina *et al.*, 2004), mixotrophic *Hydrogenophaga* sp. (Kämpfer *et al.*, 2005) and uncultured Bacteroidetes. Sequences affiliated with sulfate reducing Desulfobacterales (Kuever *et al.*, 2005), *Desulfonatronum* sp. (Zhilina *et al.*, 2005), and *Desulfovibrio* sp. (Abildgaard *et al.*, 2006), and sulfur oxidizing *Thiomicrospira* sp. (Brinkhoff and Muyzer, 1997) and *Thioalkalispira* sp. (Sorokin *et al.*, 2002) were also detected in the sediments (Figure 4). Despite variations in sediment community assemblage, sequences affiliated with thermophilic *Thermococcus mexicalis* (Lepage *et al.*, 2004), *Methanosaeta thermophila* (Kamagata *et al.*, 1992), *Pelotomaculum thermopropionicum* (Imachi *et al.*, 2002) and *Thermodesulfovibrio yellowstoni* (Henry *et al.*, 1994) were either exclusively present or more abundant in the bubbling fluid.

Functional genes in metagenome
Metagenome data with a total of 495 960, 488 597, 335 045 and 511 350 reads were obtained from sediments at 3, 13, 23 and 31 cm, respectively (Supplementary Table S4). The summed read length was roughly equivalent to a total of 583 Mbps. Abundances of the genes *mmo/pmo*, *apr* and *dsr* at 3 and 13 cm were greater than those at 23 and 31 cm (Figure 5). In contrast, abundance of the gene *mcr*

peaked at 23 cm, was maintained at a moderate level at 3 and 13 cm, and decreased to a low level at 31 cm.

Incubation experiments
Methane was produced in incubations supplied with methanogenic precursors (H_2/CO_2, acetate and methanol/methylamine) for sediments collected from all investigated depth intervals. The initial methanogenic rates for the incubations supplied with methylamine/methanol ranged between 2 to 4 nmol h^{-1} g^{-1} at 4–21 cm, and decreased to 0.5 nmol h^{-1} g^{-1} at three deepest intervals (Figure 6). The initial methanogenic rates for the incubations supplied with acetate increased with depth with high values (2 to 5 nmol h^{-1} g^{-1}) occurring at 20–30 cm, whereas those with H_2/CO_2 exhibited two peak zones near the SMTZ and at 25 cm.

Methane was aerobically consumed in incubations of sediments from all investigated depth intervals. Initial methane in headspace ($\sim 8 \times 10^4$ p.p.m.v.) was reduced to a level below 500 p.p.m.v. within 2 weeks for sediments from nearly all investigated depth intervals (except for sediments at 25 cm). As the headspace was episodically supplied with air during incubation and the internal pressure was not monitored, methane consumption rate could not be precisely calculated.

Sulfate reduction was slow in sulfate-supplied incubations of sediments from all investigated depth intervals. The addition of a mixture of yeast extract, peptone and trypton stimulated the sulfate consumption rate with added sulfate reduced to a level below 0.01 mM in 2 weeks. Incubations of sediments supplied with ^{13}C-labeled methane and sulfate did not result in the detectable production of ^{13}C-enriched CO_2 over a period of 6 months.

Modeled consumption and production rates of sulfate and methane
The reactive-transport modeling demonstrated that the net production of sulfate occurred at a rate of 5.38 mM per year within the top 6 cm. The net consumption of sulfate proceeded at a rate of
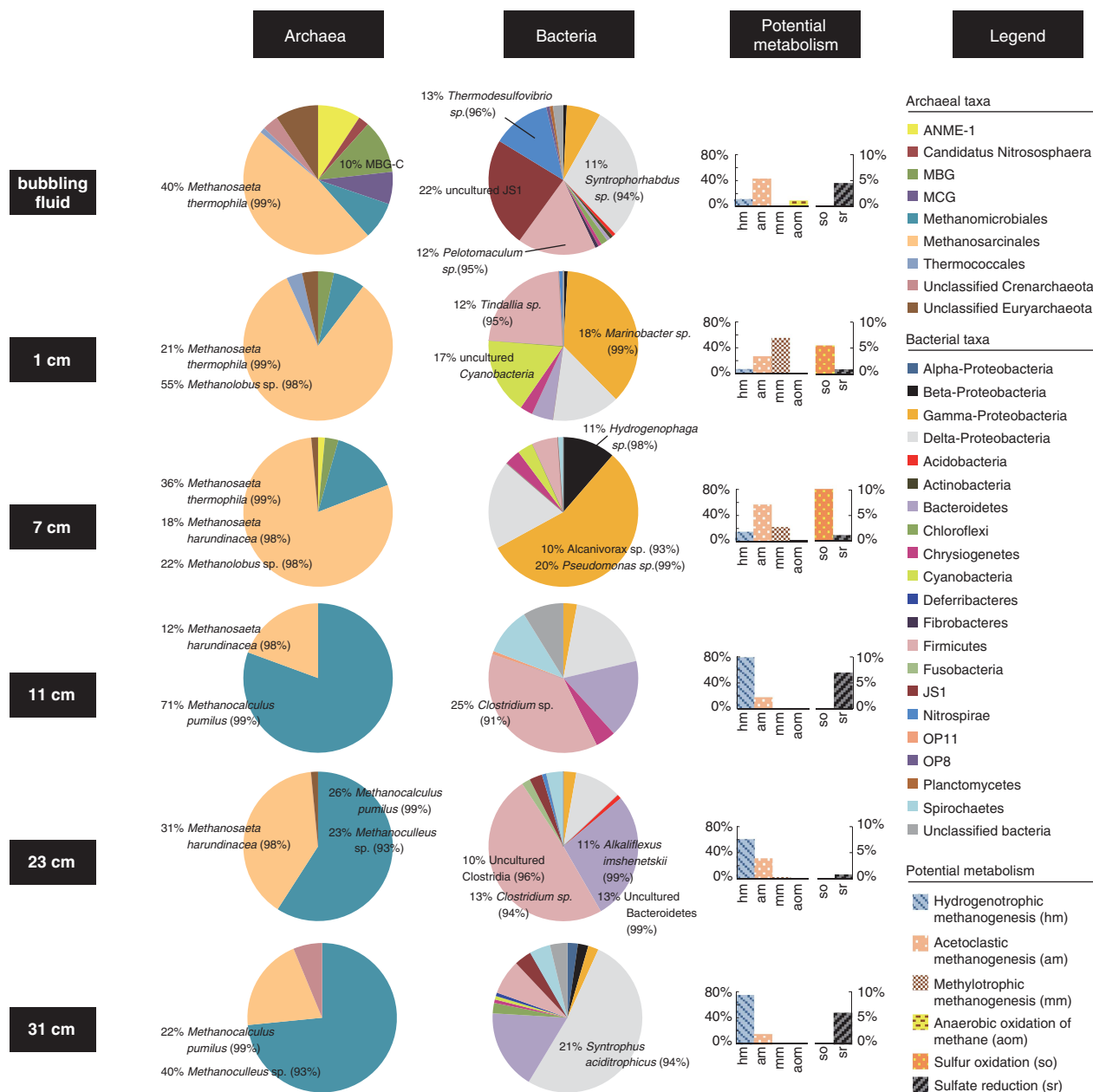
Figure 4 Bacterial and archaeal community structures in core c3 collected in 2009 based on the 16S rRNA gene analysis. Bacterial and archaeal communities are categorized by phylum and order, respectively. The fractions of the dominant phylotypes (>10% of each library), and their nearest culture representatives or environmental sequences are highlighted in the pie chart. The fractions of the phylotypes attributed to potential metabolisms (including methanogenesis, AOM, sulfate reduction and sulfur oxidation) are shown in the histograms. MBG stands for Marine Benthic Group, whereas MCG for Miscellaneous Crenarchaeal Group.

2.16 mM per year at 6–14 cm (Supplementary Figure S3) and decreased from 0.49 mM per year at 14–22 cm to nearly zero at depths further below. The integrated rate fluxes of sulfate production (or sulfide oxidation) at the top 6 cm and sulfate reduction across the SMTZ were 3.16×10^{-1} and 1.78×10^{-1} mol m^{-2} per year, respectively. For comparison, the net methane consumption occurred at a rate of 0.82 mM per year or an integrated rate flux of 1.10×10^{-1} mol m^{-2} per year at $\leqslant 14$ cm. The net methane production occurred at a rate of 0.79 mM per year or an integrated rate flux of 1.34×10^{-1} mol m^{-2} per year at $\geqslant 14$ cm. If the transition from the net sulfate production to the net sulfate consumption is assumed to be the oxic–anoxic boundary, the integrated rate flux of aerobic and anaerobic methanotrophy would be 4.33×10^{-2} and 6.66×10^{-2} mol m^{-2} per year, respectively.

Discussion

Fluid transport and surface alteration
Fluids expelled from MVs are generally considered to rapidly migrate along the fracture tapping into
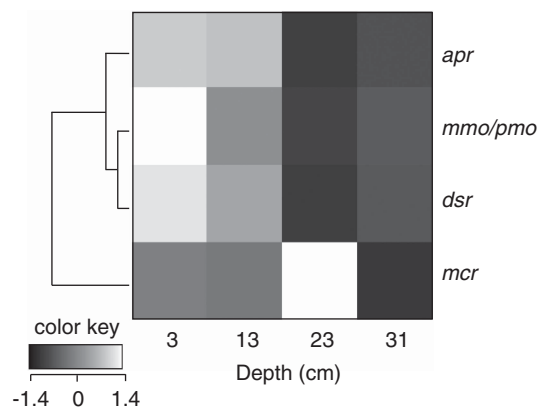
Figure 5 Heat map for pyrosequencing reads matching the genes *apr*, *dsr*, *mmo/pmo* and *mcr*. The Z-scores are scaled between − 1.4 and 1.4, and assigned with different gray scales. The lighter the gray scale is, the greater the relative gene abundance is. The distances between genes are the Euclidean distance.

Figure 6 Initial methane production rates along the depth profile for incubations supplied with methanogenic precursors. ● for H_2/CO_2; ■ for acetate; and ◆ for methylamine/methanol.

deep geological structures or reservoirs. Fluids and sediments released are subsequently deposited in the peripheral mud platform or drained toward the topographic depression, and subject to the alteration of surface processes. Therefore, fluids collected from mud pools or localized bubbling features could potentially constrain the compositions of deeply sourced fluid and surface processes. In this study, chloride conserved to microbial and most abiotic processes was first used as a tracer of fluid process. The chloride concentration in the top pore water was 1.6–1.9 times greater than that in the bubbling fluid. Such an enrichment of chloride concentration is best explained by surface evaporation. In addition, the isotopic compositions of fluids collected from the SYNHMV (Figure 1) and MVs in the adjacent areas (Supplementary Figure S1) deviated from the local meteoric water line at various degrees (Supplementary Figure S2), suggesting that these fluids are subject to the long-term water–rock interaction and surface evaporation (Wang *et al.*, 2001). The interpretation of surface evaporation based on chloride concentrations and isotopic compositions are mutually consistent with each other. Second, the chloride concentration in the bottom pore water was comparable to that in the bubbling fluid (Figures 2a and 3a), suggesting that deeply sourced fluids are relatively less saline (100–120 mM chloride), and the variation of chloride in pore water could be attributed to the mixing between the deeply sourced, dilute component and the surface, saline component. Third, the enrichment of chloride in the top pore water was much less than that of sulfate (1.6 and 9.2 times for chloride and sulfate, respectively, in core c1; 1.9 and 276 times for chloride and sulfate, respectively, in core c2), suggesting that an additional sulfur source is required to enhance the sulfate concentration. The oxidation of fine-grained sulfide minerals (such as pyrite and greigite), previously identified in the host geological formation (Horng and Roberts, 2006),
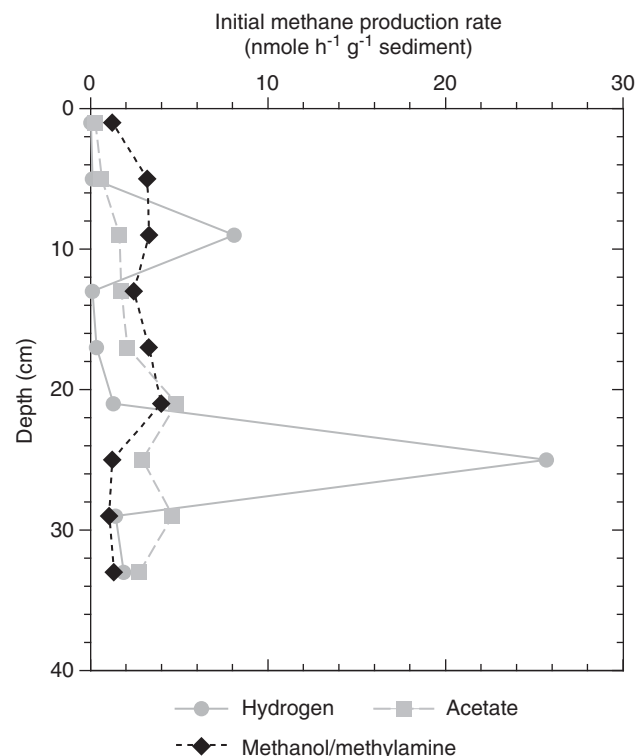
appears to be the most plausible mechanism to account for the elevated sulfate concentration at the top interval. Whether this mineral oxidation is mediated by abiotic or microbial processes remains uncertain. The sulfate produced from evaporative condensation of solute and mineral oxidation is vital for microbial sulfate reduction at depth. Finally, the magnitude of sulfate depletion in pore water was much greater than that of chloride (Figures 2 and 3). The concentration profiles for compounds susceptible to microbial metabolisms could be readily distinguished from those controlled purely by abiotic processes.

Geochemical and metabolic zonation
The geochemical results obtained in this study reveal a stratified metabolic zonation pattern. Sulfate concentrations decreased from > 0.8 mM at the top to being nearly exhausted at ∼10 cm in both cores c1 and c2 (Figures 2 and 3). The decrease of sulfate was accompanied with the increase of methane with depth, marking a SMTZ. Like those observed in marine settings (Borowski *et al.*, 1997; Treude *et al.*, 2005), the observed SMTZ and geochemical profiles suggest active sulfate reduction, AOM and methanogenesis. The interpretation of the observed profiles is further supported by the decreasing $\delta^{13}C$ values of methane with depth, the relative depletion of ^{13}C in methane in the

methanogenic zone when compared with the bubbling fluid, and the coincidence of the smallest δ^{13}C-dissolved inorganic carbon values at the SMTZ.

The geochemical and metabolic stratification is apparently persistent over years (2007 vs 2009). Although chloride concentrations in the bubbling fluids collected in 2007 and 2009 remain nearly the same, the variation magnitudes of compounds susceptible to microbial metabolisms are time-dependent. For example, sulfate concentrations were 0.8 and 4.1 mM in the top pore water obtained in 2007 and 2009, respectively (Figures 2 and 3). The difference in sulfate abundance could be accounted for by the duration of surface exposure of sediments to the atmosphere, the discharge frequency and magnitude of fluids and sediments, and the dilution caused by precipitation. Similarly, methane concentrations varied substantially within the methane-rich zone regardless of the cores analyzed, suggesting that methanogenesis is time- and depth-dependent, and heterogeneously distributed within the pore space.

Overall, surface processes and microbial activities exert a profound effect on the enrichment of sulfate in the top pore water and methane in the methane-rich zones. Despite that the exact magnitude of variation in sulfate or methane abundance and the depth of SMTZ change temporarily, the metabolic stratification is persistently maintained at the SYNHMV. This is in contrast with the iron/manganese-methane transition signifying the metal-dependent AOM in a MV of eastern Taiwan (Chang et al., 2012) and exhibits great similarities with those commonly observed in marine counterparts. The presence of such a geochemical pattern and metabolic stratification seems to link to the strong depth-dependent regulation imposed by the interactions between surface processes and subsurface fluid transport.

Stratified community assemblages and functions
The metabolic stratification inferred from geochemical profiles is consistent with the relative abundances of functional genes retrieved from the metagenome data and with the inference of 16S rRNA gene sequences from the clone libraries. First, the abundances of reads matching the *mmo/pmo* and *apr* gene sequences decreased significantly with depth (Figure 5). In addition, abundant *Alcanivorax*-, Cyanobacteria-, *Hydrogenophaga*-, *Marinobacter*- and *Pseudomonas*-related 16S rRNA gene sequences were detected at 1 and 7 cm (Figure 4), and methane was aerobically consumed in all incubations. The gene *mmo/pmo* accounts for aerobic methane oxidation, whereas the gene *apr* represents the reversible conversion between sulfite and sulfate during either dissimilatory sulfate reduction or the oxidation of elemental sulfur or sulfide. Therefore, the enhanced abundance of these two genes at shallow depths together with the presence of

sequences affiliated with oxygenic phototrophs and aerobic heterotrophs suggests that oxygen requiring microorganisms must proliferate above the transition zone where atmospheric oxygen could penetrate. Although the exact depth of oxygen penetration is not determined, the oxygen infiltrated from the atmosphere and produced by cyanobacteria would be transiently depleted by aerobic methanotrophy and/or heterotrophy, favoring the proliferation of anaerobes at depth.

In contrast, the presence of the genes *dsr* and *mcr* indicates the capability for anaerobic sulfate reduction and methanotrophy/methanogenesis, respectively. The observed relative abundances of the genes, *dsr* and *mcr*, exhibit inverse depth-dependent trends to each other (Figure 5), a pattern consistent with the geochemical interpretation that sulfate reduction and methanogenesis are primarily confined at the shallow depths and within the methane-rich zone, respectively. The metagenome data is also in part corroborated with the detection of 16S rRNA gene sequences affiliated with Desulfobacterales and Desulfovibrionales within Delta-Proteobacteria, ANME-1 members, Methanomicrobiales and Methanosarcinales (Figure 4), and with the active sulfate reduction and methane production in the incubations.

Finally, to compare the communities from individual samples, the UniFrac program (Lozupone and Knight, 2005) with the Cluster Environments algorithm for the abundance-weighted phylotypes was employed. The bacterial and archaeal communities at depths above and below the SMTZ formed distinct clusters (Figure 7). The transition of both archaeal and bacterial communities at the SMTZ is consistent with the metabolic stratification inferred from the metagenome data. Such a community relationship supports the assertion that stratified microbial functions and community structures are strongly regulated by the geochemical context imposed by the interactions between surface processes and subsurface fluid transport.

The UniFrac analysis also indicated that the community assemblage in the bubbling fluid was distinct from those associated with the sediments (Figure 7). This combined with the observation that some sequences affiliated with thermophiles were either exclusively present or more abundant in the bubbling fluid suggests that a portion of community members might be derived from a deep source at high temperatures. The exposure of sediment to the atmosphere during the fluid discharge and sediment deposition would limit the survival of these indigenous thermophilic members, whereas rendering the proliferation of mesophiles potentially capable of adapting to the oxidative stress.

The majority of methanogen-related 16S rRNA gene sequences were related to Methanosarcinales (*Methanosaeta*- and *Methanolobus*-related strains; dominating at ⩽7 cm) and Methanomicrobiales (*Methanoculleus*- and *Methanocalculus*-related strains;
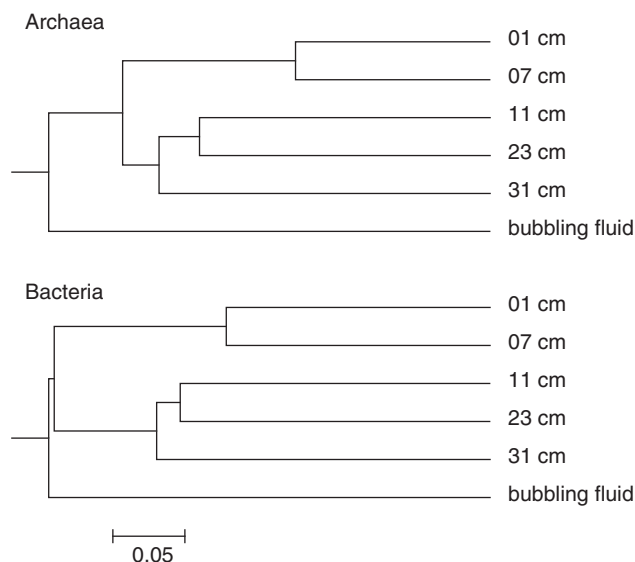
Archaea

Bacteria

0.05

Figure 7 Community clustering based on the UniFrac analysis of 16S rRNA gene clone libraries. Scale bar shows the distance between each environmental sample.

dominating at $\geqslant 11$ cm; Figure 4). *Methanolobus* obligatorily utilizes non-competitive methyl compounds produced from the fermentation of osmoprotectants (such as glycerol) in hypersaline or saline environments (Zinder, 1993; Whitman *et al.*, 2006). These methanogens could coexist with sulfate reducers without the need of substrate competition. Although the average chloride concentration in the top pore water does not exceed that of seawater, surface evaporation might lead to the local enhancement of salinity, thereby favoring the predominance of *Methanolobus*-related members at shallow depths. The activity of these methanogens would not be great, as methane is not substantially depleted in ^{13}C and methane concentrations are not enhanced at shallow depths. Methane produced *in situ* by these methanogens would be further consumed by aerobic and anaerobic methanotrophy.

Below 10 cm, where sulfate was nearly exhausted, the *Methanomicrobiales*-related members outnumbered the other methanogens and likely produced methane through CO_2 reduction. Methanogenic activities at these depth intervals are apparently high as evidenced by the high methane levels, the depletion of ^{13}C in methane and the maximum initial rates for the incubation of sediments at 25 cm with H_2/CO_2 (Figures 3 and 6). The high methanogenic activity has to be tied to the fermentative production of H_2 through a syntrophic relationship by which hydrogenotrophic methanogens and hydrogen-producing fermenters maximize the efficiency of interspecies H_2 transfer (Ishii *et al.*, 2005; Kimura *et al.*, 2010). These methanogens are most likely heterogeneously distributed within the methane-rich zone, thereby accounting for the fluctuating methane levels obtained from triplicate measurements.

Conclusions
Although metabolic stratification at the SYNHMV resembles that in marine counterparts, the driving force that charges the deeply sourced, oxidant-depleted fluids with sufficient amounts of electron acceptor is quite different. As no sulfate-rich seawater overlies sediments, the intrusion of atmospheric oxygen fuels aerobic methane/sulfide oxidation and transforms sulfide minerals into sulfate (Supplementary Figure S5). With the feedback of aerobic metabolisms, the dissolved oxygen would be transiently depleted to facilitate the colonization of anaerobes that harvest metabolic energy from either mineral-derived sulfate or organic carbon inherited in sediments. Methane flux generated by *in situ* methanogenesis appears to overprint the thermogenic methane migrating from deep sources quantitatively and isotopically, and to exceed the capacity of microbial consumption. Interpretations constrained by geochemical and molecular results demonstrate that tightly coupled carbon and sulfur cycles enable the link of deep crustal environments with surface microbial and abiotic processes in terrestrial MV ecosystems. Such surface–subsurface interactions would allow the creation of numerous micro-niches harboring various assemblages of specialized microorganisms modulated under specific geochemical contexts.

Conflict of interest

The authors declare no conflict of interest.

Acknowledgements

References

Abildgaard L, Nielsen MB, Kjeldsen KU, Ingvorsen K. (2006). *Desulfovibrio alkalitolerans* sp. nov., a novel alkalitolerant, sulphate-reducing bacterium isolated from district heating water. *Int J Syst Evol Microbiol* **56**: 1019–1024.

Alain K, Holler T, Musat F, Elvert M, Treude T, Kruger M. (2006). Microbiological investigation of methane- and hydrocarbon-discharging mud volcanoes in the Carpathian Mountains, Romania. *Environ Microbiol* **8**: 574–590.

Alazard D, Badillo C, Fardeau ML, Cayol JL, Thomas P, Roldan T *et al.* (2007). Tindallia texcoconensis sp. nov., a new haloalkaliphilic bacterium isolated from lake Texcoco, Mexico. *Extremophiles* **11**: 33–39.

Ashelford KE, Chuzhanova NA, Fry JC, Jones AJ, Weightman AJ. (2005). At least 1 in 20 16S rRNA sequence record currently held in public repositories is estimated to contain substantial anomalies. *Appl Environ Microbiol* **71**: 7724–7736.

Boetius A, Ravenschlag K, Schubert C, Rickert D, Widdel F, Gieseke A et al. (2000). A marine microbial consortium apparently mediating anaerobic oxidation of methane. Nature 407: 623–626.

Borowski WS, Paull CK, Ussler Iii W. (1997). Carbon cycling within the upper methanogenic zone of continental rise sediments: an example from the methane-rich sediments overlying the Blake Ridge gas hydrate deposits. Mar Chem 57: 299–311.

Brinkhoff T, Muyzer G. (1997). Increased species diversity and extended habitat range of sulfur-oxidizing Thiomicrospira spp. Appl Environ Microbiol 63: 3789–3796.

Chang Y-H, Cheng T-W, Lai W-J, Tsai W-Y, Sun C-H, Lin L-H et al. (2012). Microbial methane cycling in a terrestrial mud volcano in eastern Taiwan. Environ Microbiol 14: 895–908.

Etiope G, Lassey KR, Klusman RW, Boschi E. (2008). Reappraisal of the fossil methane budget and related emission from geologic sources. Geophy Res Lett 35: L09307.

Etiope G, Feyzullayev A, Baciu CL. (2009). Terrestrial methane seeps and mud volcanoes: A global perspective of gas origin. Marine Petrol Geol 26: 333–344.

Henry E, Devereux R, Maki J, Gilmour C, Woese C, Mandelco L et al. (1994). Thermodesulfovibrio yellowstonii, gen. nov. and sp. nov.: its phylogenetic relationship to Thermodesulfobacterium commune and their origins deep within the bacterial domain. Arch Microbiol 161: 62–69.

Horng C-S, Roberts AP. (2006). Authigenic or detrital origin of pyrrhotite in sediments?: Resolving a paleomagnetic conundrum. Earth Planet Sci Lett 241: 750–762.

Huber H, Hohn MJ, Rachel R, Fuchs T, Wimmer VC, Stetter KO. (2002). A new phylum of Archaea represented by a nanosized hyperthermophilic symbiont. Nature 417: 63–67.

Imachi H, Sekiguchi Y, Kamagata Y, Hanada S, Ohashi A, Harada H. (2002). Pelotomaculum thermopropionicum gen. nov., sp. nov., an anaerobic, thermophilic, syntrophic propionate-oxidizing bacterium. Int J Syst Evol Microbiol 52: 1729–1735.

Ishii Si, Kosaka T, Hori K, Hotta Y, Watanabe K. (2005). Coaggregation facilitates interspecies hydrogen transfer between Pelotomaculum thermopropionicum and Methanothermobacter thermautotrophicus. Appl Environ Microbiol 71: 7838–7845.

Kämpfer P, Schulze R, Jäckel U, Malik KA, Amann R, Spring S. (2005). Hydrogenophaga defluvii sp. nov. and Hydrogenophaga atypica sp. nov., isolated from activated sludge. Int J Syst Evol Microbiol 55: 341–344.

Kamagata Y, Kawasaki H, Oyaizu H, Nakamura K-I, Mikami E, Endo G et al. (1992). Characterization of three thermophilic strains of Methanothrix ("Methanosaeta") thermophila sp. nov. and rejection of Methanothrix ("Methanosaeta") thermoacetophila. Int J Syst Bacteriol 42: 463–468.

Kimura H, Nashimoto H, Shimizu M, Hattori S, Yamada K, Koba K et al. (2010). Microbial methane production in deep aquifer associated with the accretionary prism in Southwest Japan. ISME J 4: 531–541.

Knittel K, Boetius A. (2009). Anaerobic oxidation of methane: progress with an unknown process. Annu Rev Microbiol 63: 311–334.

Kopf AJ. (2004). Significance of mud volcanism. Rev Geophys 40: 1–52.

Kuever J, Rainey FA, Widdel F. (2005). (The Proteobacteria) part C (The Alpha-, Beta-, Delta-, and Epsilon-proteobacteria). In: Brenner DJ, Krieg NR (eds). Bergey's Manual of Systematic Bacteriology, 2 edn. Springer: New York, pp 959–987.

Lane DJ. (1991). 16S/23S rRNA sequencing. In: Stackenbrandt E, Goodfellow M (eds). Nucleic Acid Techniques in Bacterial Systematics. Wiley: NY, pp 115–175.

Lepage E, Marguet E, Geslin C, Matte-Tailliez O, Zillig W, Forterre P et al. (2004). Molecular diversity of new Thermococcales isolates from a single area of hydrothermal deep-sea vents as revealed by randomly amplified polymorphic DNA fingerprinting and 16S rRNA gene sequence analysis. Appl Environ Microbiol 70: 1277–1286.

Lin L-H, Gihring T, Sherwood Lollar B, Boice E, Pratt L, Lippmann-Pipke J et al. (2006). Planktonic microbial communities associated with fracture-derived groundwater in a deep gold mine of South Africa. Geomicrobiol J 23: 475–498.

Lozupone C, Knight R. (2005). UniFrac: a new phylogenetic method for comparing microbial communities. Appl Environ Microbiol 71: 8228–8235.

Milkov AV. (2004). Global estimates of hydrate-bound gas in marine sediments: how much is really out there? Earth-Sci Rev 66: 183–197.

Orphan VJ, House CH, Hinrichs K-U, McKeegan KD, DeLong EF. (2002). Multiple archaeal groups mediate methane oxidation in anoxic cold seep sediments. Proc Natl Acad Sci 99: 7663–7668.

Qiu Y-L, Hanada S, Ohashi A, Harada H, Kamagata Y, Sekiguchi Y. (2008). Syntrophorhabdus aromaticivorans gen. nov., sp. nov., the first cultured anaerobe capable of degrading phenol to acetate in obligate syntrophic associations with a hydrogenotrophic methanogen. Appl Environ Microbiol 74: 2051–2058.

RDC Team (R Development Core Team) (2008). R: A language and environment for statistical computing. R Foundation for Statistical Computing: Vienna, Austria.

Shiratori H, Sasaya K, Ohiwa H, Ikeno H, Ayame S, Kataoka N et al. (2009). Clostridium clariflavum sp. nov. and Clostridium caenicola sp. nov., moderately thermophilic, cellulose-/cellobiose-digesting bacteria isolated from methanogenic sludge. Int J Syst Evol Microbiol 59: 1764–1770.

Sorokin DY, Tourova TP, Kolganova TV, Sjollema KA, Kuenen JG. (2002). Thioalkalispira microaerophila gen. nov., sp. nov., a novel lithoautotrophic, sulfur-oxidizing bacterium from a soda lake. Int J Syst Evol Microbiol 52: 2175–2182.

Sun C-H, Chang S-C, Kuo C-L, Wu J-C, Shao P-H, Oung JH. (2010). Origins of Taiwan's mud volcanoes: evidence from geochemistry. J Asian Earth Sci 37: 105–110.

Treude T, Niggemann J, Kallmeyer J, Wintersteller P, Schubert C, Boetius A et al. (2005). Anaerobic oxidation of methane and sulfate reduction along the Chilean continental margin. Geochim Cosmochim Acta 69: 2767–2779.

Wang B, Lai Q, Cui Z, Tan T, Shao Z. (2008a). A pyrene-degrading consortium from deep-sea sediment of the West Pacific and its key member Cycloclasticus sp. P1. Environ Microbiol 10: 1948–1963.

Wang CH, Kuo CH, Peng TR, Chen WF, Liu TK, Chiang CJ et al. (2001). Isotope characteristics of Taiwan groundwaters. West Pac Earth Sci 1: 415–428.

Wang G, Spivack AJ, Rutherford S, Manor U, D'Hondt S. (2008b). Quantification of co-occurring reaction rates in deep subseafloor sediments. *Geochim Cosmochim Acta* **72**: 3479–3488.

Whiticar MJ. (1990). A geochemical perspective of natural gas and atmospheric methane. *Org Geochem* **16**: 531–547.

Whitman W, Bowen T, Boone D. (2006). The methanogenic bacteria. In: Dworkin M, Falkow S, Rosenberg E, Schleifer K-H, Stackebrandt E (eds) *The Prokaryotes*, 3rd edn. Springer-Verlag: New York, pp 165–207.

Wrede C, Brady S, Rockstroh S, Dreier A, Kokoschka S, Heinzelmann SM *et al.* (2012). Aerobic and anaerobic methane oxidation in terrestrial mud volcanoes in the Northern Apennines. *Sediment Geol* **263–264**: 210–219.

Zhang W, Xue Y, Ma Y, Grant WD, Ventosa A, Zhou P. (2002). *Marinospirillum alkaliphilum* sp. nov., a new alkaliphilic helical bacterium from Haoji soda lake in Inner Mongolia Autonomous Region of China. *Extremophiles* **6**: 33–37.

Zhilina TN, Appel R, Probian C, Brossa EL, Harder J, Widdel F *et al.* (2004). *Alkaliflexus imshenetskii* gen. nov. sp. nov., a new alkaliphilic gliding carbohydrate-fermenting bacterium with propionate formation from a soda lake. *Arch Microbiol* **182**: 244–253.

Zhilina TN, Zavarzina DG, Kuever J, Lysenko AM, Zavarzin GA. (2005). *Desulfonatronum cooperativum* sp. nov., a novel hydrogenotrophic, alkaliphilic, sulfate-reducing bacterium, from a syntrophic culture growing on acetate. *Int J Syst Evol Microbiol* **55**: 1001–1006.

Zinder SH. (1993). Physiological ecology of methanogens. In: Ferry JG (ed) *Methanogenesis: Ecology, Physiology, Biochemistry and Genetics.* Chapman and Hall: New York, pp 128–206.

Supplementary Information accompanies the paper on The ISME Journal website (http://www.nature.com/ismej)